Indian Journal of Pure & Applied Physics
Vol. 58, December 2020, pp. 864-876

Electrochemical and lithium-ion transport properties of layered Li-rich $Li_{1.10}(Ni_{0.32}X_{0.01}Co_{0.33}Mn_{0.33})O_2$ (X = Dy/Gd/Ho) positive electrodes

P Senthil Kumar[a], A Sakunthala[b#*], M V Reddy[c,d,e], R Prasada Rao[d], B V R Chowdari[c,d] & S Adams[d]

[a]Department of Chemical Engineering, National Taiwan University, Taipei, Taiwan 10617, ROC

[b]Department of Physics, Karunya Institute of Technology and Sciences, Coimbatore 641 114, Tamil nadu, India

[c]Department of Physics, Advanced Batteries Lab, National University of Singapore, Singapore 117 542

[d]Department of Materials Science and Engineering, National University of Singapore, Singapore 117 542

[e]Centre of Excellence in Transportation Electrification and Energy Storage (CETEES), Hydro-Québec, Canada

Received 23 March 2020; accepted 15 October 2020

Layer structured $Li_{1.10}(Ni_{0.32}X_{0.01}Co_{0.33}Mn_{0.33})O_2$ (X = Dy/Gd/Ho) compounds were synthesized via the microwave assisted solvothermal route. The impacts of doping on the electrical and electrochemical properties of $Li_{1.10}(Ni_{0.32}X_{0.01}Co_{0.33}Mn_{0.33})O_2$ compounds were investigated. Rietveld refined XRD pattern showed $Li_{1.10}(Ni_{0.32}X_{0.01}Co_{0.33}Mn_{0.33})O_2$ compounds with layered hexagonal structure. SEM images revealed the compounds with micrometer sized grains. The $Li_{1.10}(Ni_{0.33}Co_{0.33}Mn_{0.33})O_2$ compound delivered an initial discharge capacity of 197 mAh/g at 0.2C and retained a capacity of 163mAh/g after 50th cycle in the voltage window of 2.5-4.6V. The cycling stability of $Li_{1.10}(Ni_{0.33}Co_{0.33}Mn_{0.33})O_2$ compound was improved with rare earth doping. $Li_{1.10}(Ni_{0.32}Dy_{0.01}Co_{0.33}Mn_{0.33})O_2$ compound delivered the discharge capacity of 166 mAh/g after50th cycle in the potential window 2.5-4.6V at 0.2C with 100% capacity retention. AC impedance studies displayed the electrical conductivity in the order of 10^{-6} S/cm. Wagner polarization analysis revealed the improvement in electronic transference number *via* rare earth doping.

Keywords: lithium ion battery, cathode, excess lithium, microwave, rare earthdoping

1 Introduction

High voltage cathode materials are in great demand in order to develop higher energy density lithium ion batteries[1-12].Among several high capacity ternary oxides, the lithium nickel cobalt manganese oxide, $Li(Ni_{0.33}Co_{0.33}Mn_{0.33})O_2$ has received a considerable attention due to its excellent properties such as low cost, high safety and high reversible capacity since it was first proposed by Ohzuku *et al.*[13]. But, it has some drawbacks such as poor cycling stability due to the cationic exchange between Li^+/Ni^{2+}ions and by its poor electrical conductivity[14]. Hence, in order to improve its performance various preparation conditions were considered and reported in literatures[15-17]. Cedar *et al.*[18] and Levasseur *et al.*[19] reported that the excess lithium in layered $LiCoO_2$ impacts its electrochemical properties. Similarly, the effect of excess lithium in layered $LiNi_{0.5}Mn_{0.5}O_2$ was studied by Myung *et al.*[20] and Shlyakhtin *et al.*[21]. Though they did not find any significant difference in the crystal structure between stoichiometric and non-stoichiometric compounds, the electrochemical properties were improved by excess lithium. Following the above reports, the electrochemical properties of excess lithium in Li $(Ni_{0.33}Co_{0.33}Mn_{0.33})O_2$compounds were suggested by Todorov *et al.*[22], which resulted in good electrochemical properties. However, the basis of the improved electrochemical properties by excess lithium was not clarified by any authors.Recently our group studied the structural, electrical and electrochemical characteristics of lithium excess $Li_{1+x}(Ni_{0.33}Co_{0.33}Mn_{0.33})O_2$ (x=0/0.05/ 0.10/0.15/0.20 mol) compounds[23].We found that there was no large difference in the lattice parameters and in the electrical conductivity (10^{-6} S/cm) observed. However, the specific charge/discharge capacity and cycling stability of the lithium excess compound $Li_{1.10}(Ni_{0.33}Co_{0.33}Mn_{0.33})O_2$ was found superior than the stoichiometric compound $LiNi_{0.33}Co_{0.33}Mn_{0.33}O_2$.

Few reports were seen on the influence of rare earth doping on stoichiometric $LiNi_{0.33}Co_{0.33}Mn_{0.33}O_2$ compound, as below. Ding *et al.*[24] reported on $Li(Ni_{1/3}Co_{1/3}Mn_{1/3})_{1-x}X_xO_2$ (X = La/Ce/Pr) materials and discussed on improved discharge capacity and cycling stability due to rare earth doping. Zhong *et al.*[25] and Ding *et al.*[26] investigated the effect of

Corresponding author:
(E-mail: meetsaku@gmail.com, *sakunthala@karunya.edu)

cerium (Ce) and lanthanum (La) on the electrochemical characteristics of $Li(Ni_{1/3}Co_{1/3}Mn_{1/3})O_2$, respectively. But, to the best of our knowledge, there was no literature found on the impact of rare earth doping in lithium excess layered structured $Li_{1+x}(Ni_{0.33}Co_{0.33}Mn_{0.33})O_2$ compounds. Hence, in this work, we have prepared a series of lithium excess cathode materials $Li_{1.10}(Ni_{0.32}X_{0.01}Co_{0.33}Mn_{0.33})O_2$ (X = Dy/Gd/Ho) for lithium ion battery. The intention of this paper is to study the influence of lanthanide elements on the structural, electrical and electrochemical performances of the lithium excess $Li_{1.10}(Ni_{0.32}X_{0.01}Co_{0.33}Mn_{0.33})O_2$ (X = Dy/Gd/Ho) cathode materials and hence to find the role of dopants.

2 Materials and Methods

Layer structured $Li_{1.10}(Ni_{0.32}X_{0.01}Co_{0.33}Mn_{0.33})O_2$ (X = Dy/Gd/Ho) compounds were synthesized via the microwave assisted solvothermal method and the preparation method was reported in our earlier reports[23].Lithium acetate, nickel acetate, manganese acetate, cobalt acetate and rare earth oxides were used as starting materials. The sample codes were fixed as **NMC**($Li_{1.10}(Ni_{0.33}Co_{0.33}Mn_{0.33})O_2$), **NMCD** ($Li_{1.10}(Ni_{0.32}Dy_{0.01}Co_{0.33}Mn_{0.33})O_2$), **NMCG** ($Li_{1.10}(Ni_{0.32}Gd_{0.01}Co_{0.33}Mn_{0.33})O_2$) and **NMCH** ($Li_{1.10}(Ni_{0.32}Ho_{0.01}Co_{0.33}Mn_{0.33})O_2$) for bare and doped compounds, respectively.

The phase purity of the product was studied by X-Ray Diffractometer (Bruker D8) with Cu K_α-adiation in the 2θ range 10-80^o at a scan rate of 0.02^o s^{-1}.TOPAS 4.2 was used for the refinement. The surface morphology was examined using SEM (JEOL JSM-6700F). MALVERN Zeta sizer ZS-90 particle size analyser was used for analysing the particle size. Tristar 3000 (Micromeritics USA) was used for measuring BET surface area of the powders. Raman analysis was carried out using Raman spectrometer (Model Lab ram HR Evolution, Horiba Scientific) with λ = 514 nm, and power of 100 mW.XPS studies were made using AXIS ultra DLD spectrometer with monochromatic Al K_α radiation (KratosAnalytica) in the ranges 0 - 1200 eV, and Casa XPS software was used to analyse XPS spectral data.

The electrical conductivity of the as prepared powder materials were calculated by AC impedance spectroscopy techniques using CH-Instrument within the range of 40 Hz - 1MHz at ambient temperature. Amplitude voltage was fixed as 50 mV. Wagner polarization analysis and DC conductivity was calculated by a *Keithley* 4001 source meter and 4-probe instruments, respectively. Galvanostatic charge-discharge and cyclic voltammetry (CV) studies were carried out with fabricated 2016 size coin cells in Arfilled glove box (MBraun, Germany). The lithium metal was used as the reference and 1 M $LiPF_6$ in EC and DMC (1:1, *v/v*) (Merck) as the electrolyte. The slurry was prepared by mixing 70% prepared cathode powder with 15% Super P conductive carbon black and 15% PVdF (Kynar 2801) in N-methylpyrrolidone, which was coated on aluminium foil. The charge discharge analysis and CV studies were examined using a Bitrode multiple battery testers (Model SCN, Bitrode, USA) and Macpile II (Biologic, France), respectively.

3 Results and Discussion

In order to verify the hexagonal layered structure of the obtained $Li_{1.10}(Ni_{0.32}X_{0.01}Co_{0.33}Mn_{0.33})O_2$ (X = Dy/Gd/Ho) compounds and to identify the percentage of Li^+/Ni^{2+} cation exchange, a Rietveld refinement was executed based on the powder XRD pattern as given in Fig. 1(a-d).The crystalline structure based on the layered α-$NaFeO_2$ structurewith space group R*3-m*, was used for refinement. During the refinement, the tenancy of the 3*a* sites by Co and Mn was stable as 0.33 for each ion. The total amount of Li and Ni was also observed to be static. All the diffraction peaks were relatively narrow revealing good crystalinity of the compounds. Good crystalline nature ensures the formation of the oxide. All the compounds show well clear peak splitting at the plane (006/012) and (018/110), which indicate well-ordered layer structure.

A trace amount of Dy_2O_3, Gd_2O_3 and Ho_2O_3 phase was also observed around 2θ ~ 30^o for the samples NMCD, NMCG and NMCH, respectively. The calculated lattice parameters are presented in Table 1. The crystal parameter '*a*' and '*c*' values were found to be increased due to doping and closely matched with the previous reports[27-30]. A significant change was observed in cell volume, which may be ascribed to the higher ionic radii of the dopants ($Dy^{3+}/Gd^{3+}/Ho^{3+}$) than (Ni^{2+}) host ions. This significant change in cell volume is expected to improve the cycling stability of cell, as to be discussed under electrochemical studies. Increase in cell volume paves way for easy movement of lithium ions which will lead to increase in electrical conductivity and hence the electrochemical performance. In all the cases, the integrated intensity ratio (I_{003}/I_{104}) was calculated to be around~ 1.2, resulting in lower cation mixing of the compounds. The lower the cation mixing better would be the pathway for the lithium ion movement. The presence of Ni ions in place

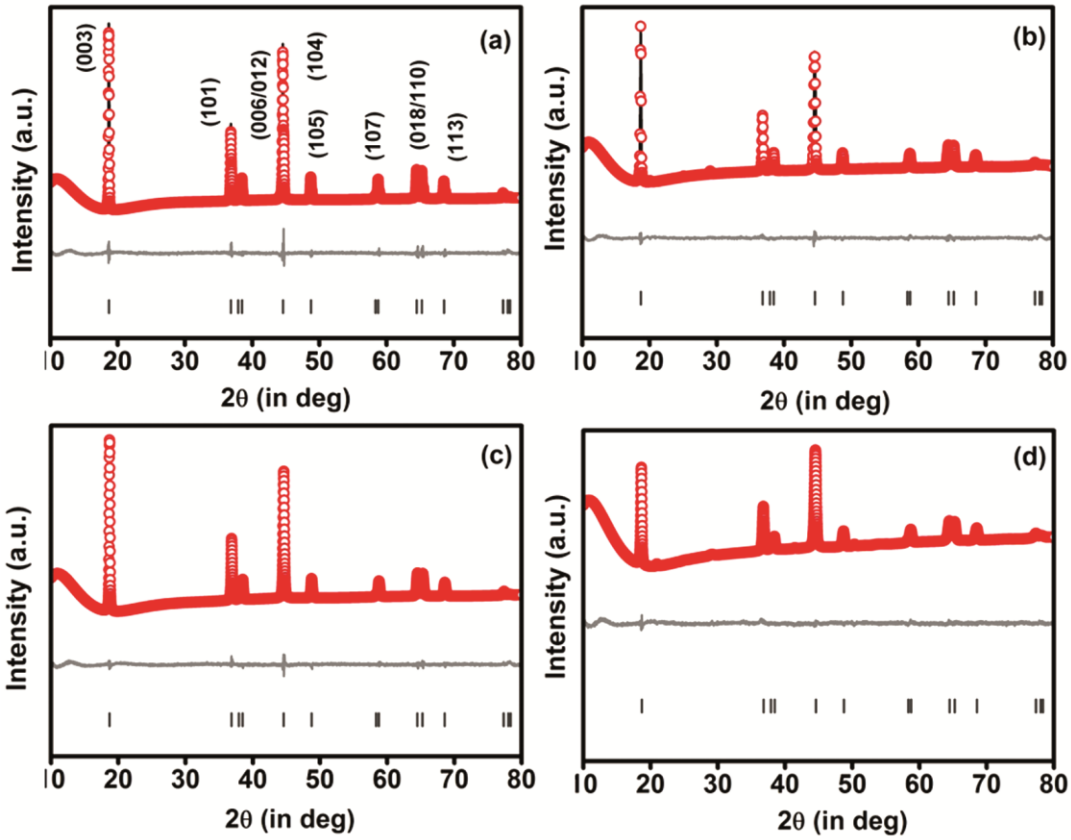

Fig. 1 — Rietveld refined XRD profiles of a) NMC, b) NMCD, c) NMCG & d) NMGH samples

Table 1 — Comparison of Rietveld Refined XRD lattice parameters

Sample code	*a* (Å)	*c* (Å)	V (Å)^3	surface area (m^2/g) (± 0.01)	Average particle size (nm)
NMC	2.841	14.145	98.82	0.85	288
NMCD	2.848	14.185	99.65	0.65	515
NMCG	2.853	14.205	100.15	0.34	570
NMCH	2.845	14.167	99.26	0.11	776

lithium sites will block the pathway for the lithium ion movement through the lattice. This indicates that the method adopted for the preparation of material favours the cation ordering. On comparison, the sample NMCD has higher I_{003}/I_{104} value which shows that doping reduces the cation exchange. The '*c/a*' ratio was found to be around ~ 4.98 for all the compounds under study revealing better hexagonal layer structure. This indicates the formation of better layered structure.

The SEM images of the samples NMC, NMCD, NMCG and NMCH are shown in Fig. 2(a). The sample NMC shows that it has polyhedral shaped particles with less agglomeration in its surface. Whereas, the samples NMCD, NMCG and NMCH have shown highly agglomerated irregular bulk particles along its surface. Among the doped samples, NMCD shows lower particle size. Particle size distribution spectra are depicted in Fig. 2(b) and the average particle size are given in Table 1 along with BET surface area. The average particle size distribution was found to be 288 nm for the sample NMC. The particle size distribution was 515, 570 and 776 nm for the samples NMCD, NMCG and NMCH, respectively. The BET surface area was found to be 0.85 m^2/g for the sample NMC and the surface area of NMCD, NMCG and NMCH samples were observed to be 0.65, 0.34 and 0.11 m^2/g, respectively.

To further investigate the crystal structure of the samples Raman scattering measurements were carried out on the prepared powder samples and the spectra are shown in Fig. 3. The sample NMC shows two

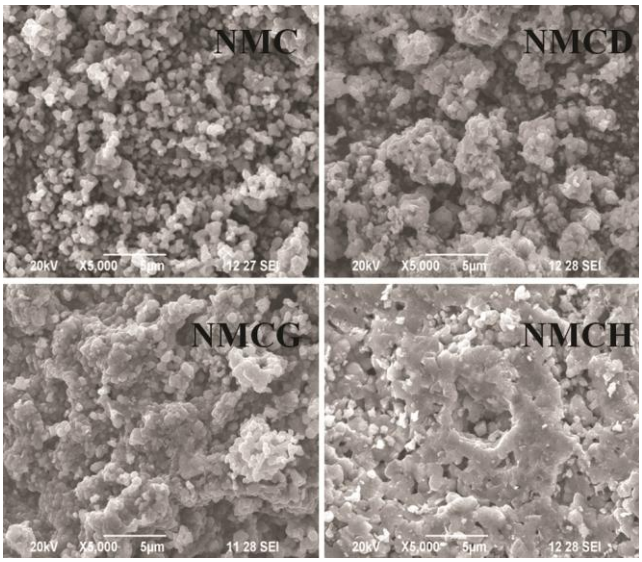

Fig.2(a) — SEM images of samples NMC. (copyright permission from Elsevier Ref .23)

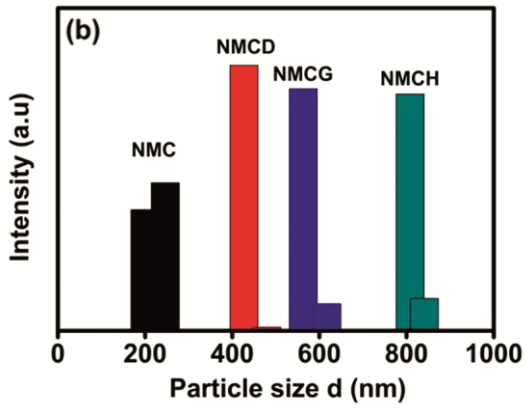

Fig. 2(b) — Particle size distribution spectra of samples NMC, NMCD, NMCG and NMCH

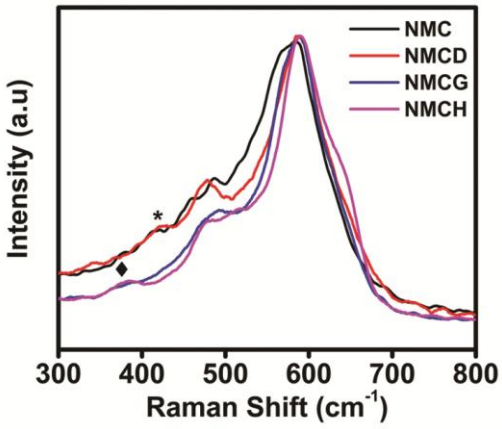

Fig. 3 — Raman spectra of NMC, NMCD, NMCG and NMCH samples

Raman bands around 585 and 485 cm^{-1}corresponding to M-O bond vibration (M = Ni/Co/Mn) leading to Raman active vibrational modes of $A_{1g}$and $E_{g,}$ respectively. For the samples NMCD, NMCG and NMCH, A_{1g} and E_g bands were observed around 590 and 478 cm^{-1}, respectively[23]. In the case of doped samples, the band corresponding to E_g mode had shifted to lower wave number when compared to sample NMC and this was attributed to the decrease in Ni-O covalency upon doping. In the case of samples NMC and NMCD, a broad weak band (indicated by * symbol) located around 420 cm^{-1} was attributed to Li_2MnO_3 superlattice, whereas the weak band located at 370 cm^{-1} (indicated by diamond symbol) for the sample NMCH was attributed to Re_2O_3 phase. Overall, Raman spectra reconfirm the hexagonal layered structure of the bare and doped compounds.

The assembled coin cells made with NMC, NMCD, NMCG and NMCH samples were tested at a current density of 0.2 C rate in different voltage ranges 2.5 to 4.4V, 2.5 to 4.6 V and 2.5 to 4.8 V at room temperature. The initial charge discharge profiles and cycling stability plot for all the samples are shown in Fig. 4 (a & b), respectively, in a

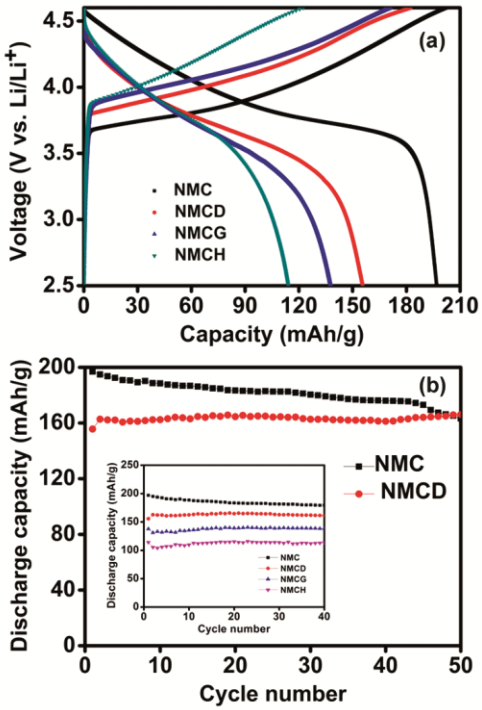

Fig. 4(a) — Charge-discharge curve and (b) cycling stability curves of the cells made with NMC, and NMCD samples in the voltage range 2.5 – 4.6 V (inset: cycling stability curves of the cells made with NMC, NMCD, NMCG and NMCH samples in the voltage range 2.5 – 4.6 V)

potential window of 2.5 to 4.6 V. The sample NMC delivers an initial specific discharge capacity of 197 mAh/g. The doped samples NMCD, NMCG and NMCH possess first cycle specific discharge capacity of 156, 138 and 114 mAh/g, respectively. The discharge capacity values at various cycles are given in Table 2. The sample NMC exhibited a lower cell polarization than that of the doped compounds. This may be due to the presence of small percentage of Dy_2O_3, Gd_2O_3 and Ho_2O_3, in case of NMCD, NMCG, and NMCH, respectively. All the samples exhibit single charge/discharge voltage plateau region (~ 3.7 V), which was consistent with the CV results, to be discussed later. On comparison, the initial irreversible capacity (ICL) was lower (~5 mAh/g) for the samples NMC, and NMCH. The ICL value was found to be 25 and 33 mAh/g for the samples NMCD and NMCG, respectively.

As seen from the Fig. 4(b) and Table. 2, the sample NMC delivers the first cycle discharge capacity of 197mAh/g and gives 176 mAh/g at the end of 40^{th} cycle with 93 % capacity retention in 2.5 – 4.6 V range. The samples NMCD, NMCG and NMCH deliver the initial discharge capacities of 151, 138 and 114 mAh/g, respectively. The sample NMCD, NMCG and NMCH deliver the discharge capacities of 161, 138 and 113 mAh/g at the end of 40^{th} cycle. The capacity retention after 40^{th} cycle was found to be 100 % for all the doped samples. In comparison with sample NCMD, sudden drop in discharge capacity was found for the sample NCM after 40^{th}cycles. The specific discharge capacity was found to be 163 mAh/g and 166 mAh/g for the samples NMC and NMCD, respectively at the end of 50^{th} cycle. This may be ascribed with the enhancement in the electronic conduction for the later one.

The galvanostatic cycling behavior of the samples NMC, NMCD, NMCG and NMCH in 2.5 – 4.4/4.8 V range at a current rate of 0.2 C are shown in Fig. 5(a & b), respectively. The initial cycle discharge capacities was found to be 170, 105, 82 and 87 mAh/g in 2.5 – 4.4 V range for the samples NMC, NMCD, NMCG and NMCH, respectively. The capacity retention was found to be 94 % for the sample NMC, whereas all the doped samples deliver excellent capacity retention of 100 % at the end of 40^{th} cycle. This indicates the importance of doping for the structural stabilization of the compound under investigation. This was mainly due to the increased volume of the unit cell as observed from the lattice parameters, as discussed under the XRD analysis. When the volume of the unit cell increases, it paves way for the easy intercalation and deintercalation of lithium ions, and hence the structural stability was maintained by doping. Similarly, the initial cycle discharge capacities was found to be 257, 174, 160 and 161 mAh/g in 2.5 – 4.8 V range for the samples NMC, NMCD, NMCG and NMCH, respectively. The

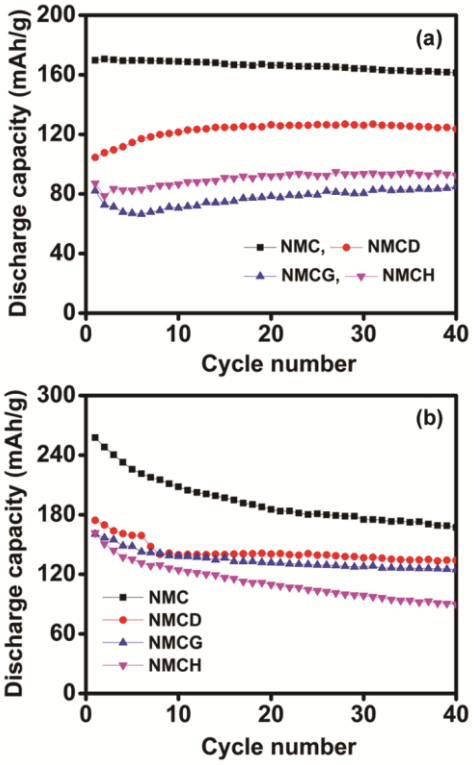

Fig. 5 — Cycling stability graphof the cells made with NMC, NMCD, NMCG and NMCH samples in the voltage range (a) 2.5 – 4.4 Vand (b)2.5 – 4.8 V

Table 2 — Comparison of Discharge capacity

Sample code	Discharge capacity (mAh/g) (± 3 mAh/g) Voltage range: 2.5-4.6 V at 30 mA/g						Capacity retention (%)
	1^{st} cycle	5^{th} cycle	10^{th} cycle	20^{th} cycle	40^{th} cycle	50^{th} cycle	
NMC	197	191	188	183	176	163	93
NMCD	156	161	162	165	161	166	100
NMCG	138	133	135	139	138	137	99
NMCH	114	107	110	115	113	110	98

capacity retention was found to be 64 % for the sample NMC, whereas all the doped samples deliver excellent capacity retention of 80 % at the end of 40th cycle. In all the cases (2.5 – 4.4/4.6/4.8 V),though the initial discharge capacity of all the doped samples are lower than that of NMC, better capacity retention has been obtained at the end of 40th cycle even at higher potential window. This indicates that rare earth doping suppress the capacity fading. The reason for the improved cycling stability was due to the enhancement in electronic conductivity upon doping, which is to be discussed in electrical studies section.

To understand the electrode kinetics of the prepared layered oxide materials cyclic voltammetry studies were carried out. The second cycle CV plots for the CR2016 coin cells made with the samples NMC and NMCD/NMCG/NMCH in a potential window of 2.5 to 4.4 V at a scan rate of 0.058 mV/s are displayed in Fig. 6(a & b), respectively. In the case of NMC, the anodic and the cathodic peaks were observed at 3.85 and 3.73/3.55 V, respectively. The observed anodic and cathodic peaks were due to the electrochemical active participation of Ni^{2+}(Ni^{2+}/Ni^{4+} redox) ions[23]. The anodic peaks were broader in nature and shifted to higher potential 4.07 V and 4.15 V for the samples NMCD and NMCG/MNCH, respectively, which was corresponding to the redox behavior of Co^{3+}/Co^{4+}. Whereas the two cathodic peaks observed at 3.73/3.55 V in NMC were merged as a single broad peak around 3.66 V for the doped samples, which was corresponding to the reduction of Ni^{4+} ions. In the case of NMCD/NMCG/NMCH, a weak broad oxidation peak was observed around 3.36 V, which was due to the oxidation of Mn^{3+}/Mn^{4+} ions. Overall, CV result indicates that rare earth doping enhanced the electrochemical participation of transition metal ions Ni^{2+}/Co^{3+}, but doping significantly reduced the reversibility of the NMC sample. Also doping changed the oxidation state of the manganese ions in $LiNi_{1/3}Co_{1/3}Mn_{1/3}O_2$ compound, which is to be discussed in XPS analysis part. These findings are consistent with the lower discharge capacity with excellent cycling stability of the doped compounds.

Bulk resistance of the prepared pellet sample was measured using AC impedance techniques in the frequency range of 1 MHz – 40 Hz at ambient temperature. The cole-coleand frequency dependent conductivity spectra of the samples NMC, NMCD, NMCG and NMCH are shown in Fig. 7(a & b), respectively. In Fig. 7(a), the sample NMC shows two regions: semicircle arc followed by inclined line. High frequency semicircle arc was related to the parallel combination of RC element and spike region was related to the effect of bulk electrodes[31-32]. In the case of samples NMCD/NMCG/NMCH, it shows

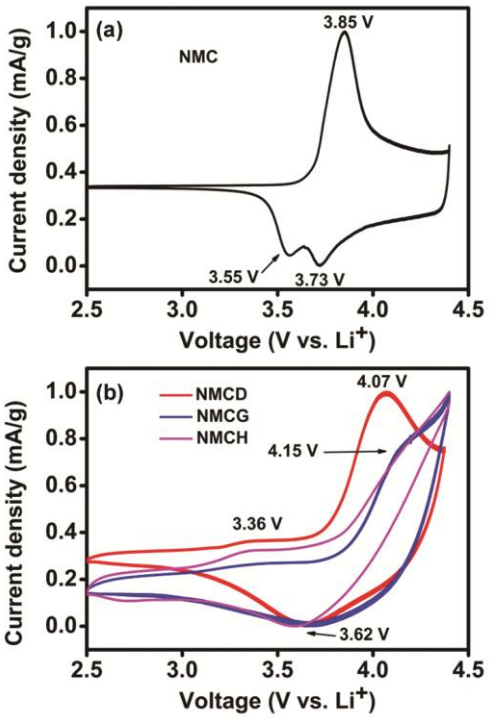

Fig. 6 — Cyclic voltammograms of the cells made with (a)NMC and (b) NMCD, NMCG and NMCH samples in the voltage range 2.5 – 4.4 V at 0.058 mV/s

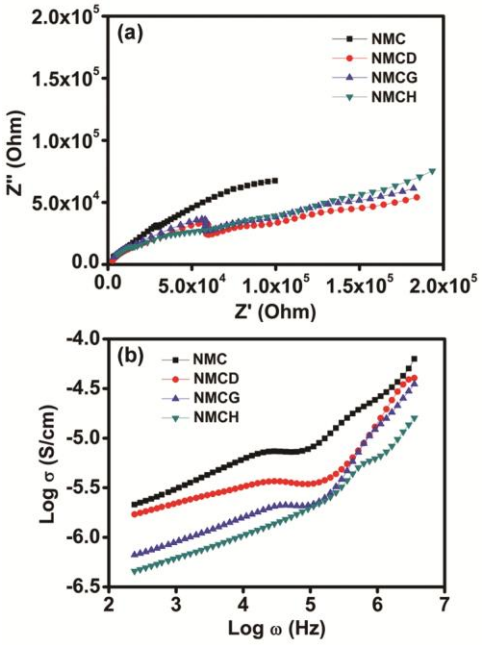

Fig. 7 — (a) Nyquist plot & (b) conductivity spectra of NMC, NMCD, NMCG and NMCH samples

high frequency suppressed semicircle along with low frequency semicircle arc, which was due to the effect of grain and grain boundary region. The bulk resistance (R_b) was calculated using the intercept of the low frequency region on the x-axis, and it was found to be 15 kΩ for the sample NMC. The bulk resistance was found to be 38, 40 and 45 kΩ for the samples NMCD, NMCG and NMCH, respectively. The electrical conductivity was measured using the relation $\sigma = (L/R_bA)$, where 'L' is the thickness and 'A' is the area of the pellet specimen. The total electrical conductivity values are given in Table 3.

In Fig. 7(b), all the samples show three regions: dispersion at low frequency range, plateau at mid frequency followed by dispersion at high frequency region. The mid frequency section characterizes dc conductivity of the specimen and it was calculated by extrapolating the plateau to y-axis. The electrical conductivity values are presented in Table 3, and the values were accorded with the Nyquist plot results. In both cases, NMC delivers higher electrical conductivity than other compounds which was due to the lower particle size and absence of impurity phase of the compound, resulting in highest discharge capacity as discussed earlier.

Hall studies were carried out to compare the 2-probe electrical conductivity with 4-probe DC conductivity and the values are given in Table 3. The 4-probe DC electrical conductivity values closely match with the results obtained from 2-probe AC impedance analysis. This validates our measurements. Ionic and electronic contribution to the total electrical conductivity was calculated by Wagner polarization method and the values are given in Table 3.Overall electrical conductivity of all the compounds was found to be in the order of 10^{-6} S/cm, but the proportion of conductivity contributed by the ionic and electronic conduction were observed to change in each compound. The ionic and electronic transference number was found to be 0.56 and 0.44 for the sample NMC. Whereas, the ionic and electronic transference number was found to be 0.54:0.46, 0.53:0.47 and 0.51:0.49 for the samples NMCD, NMCG and NMCH, respectively. This reveals that the improvement in mixed conducting nature of the NMC due to the volume expansion *via* rare earth doping and hence resulted in excellent electrochemical stability of the cells made with NMCD/NMCG/NMCH as discussed in cycling behavior.

To analyze the elemental oxidation state of the prepared powder samples NMC, NMCD, NMCG and NMCH, XPS studies was carried out. Figure 8(a-d) shows the XPS spectra of Ni2$p_{3/2}$, Mn2$p_{3/2}$, Co2$p_{3/2}$, O1*s* and Li1*s* of pristine NMC, NMCD, NMCG and NMCH samples, respectively. Figure 8(e (i-iii)) shows the XPS spectra of Dy4$d_{3/2}$, Gd4$d_{3/2}$ and Ho4$d_{3/2}$ for the samples NMCD, NMCG and NMCH, respectively. The main binding energy of Ni2$p_{3/2}$ was located at 854.85, 854.62, 854.58 and 854.89 eV for the samples NMC, NMCD, NMCG and NMCH, respectively. The main binding energy of Co2$p_{3/2}$ and Mn2$p_{3/2}$ were located at 779.92, 779.71, 779.89, 779.75 eV and 642.08, 642.05, 642.33, 642.27 eV for the samples NMC, NMCD, NMCG and NMCH, respectively. As for the B.E. of O1speaks one peak was located around 529 eV, which was corresponding to the lattice oxygen M-O (M = Ni/Co/Mn), while another peak was located around 531 eV indicated the existence of surface hydroxyls[33-35]. On comparison, the samples NMCH have high intensity O1*s* peak at 531 eV, resulting in very lower discharge capacity as discussed earlier.

The main binding energy of Li1*s* was observed as a broad and weak signal around 54 eV for all the compounds. The observed main binding energy values of Ni2$p_{3/2}$, Mn2$p_{3/2}$, Co2$p_{3/2}$, O1*s* and Li1*s* closely match with the literatures[36-39]. The XPS spectra of Ni2$p_{3/2}$ show two satellite peaks (S1 and S2) in all the samples, which was related to the Ni^{2+} ions in nickel based oxide materials. The XPS spectra of Dy4$d_{3/2}$, Gd4$d_{3/2}$ and Ho4$d_{3/2}$ peaks were observed as a weak signal in terms of intensity due to the low level of doping and confirm the 3+ oxidation state of the rare earth compounds[40]. In the case of NMCD,

Table 3 — Comparison of Electrical conductivity

Sample code	Conductivity (S/cm) (± 0.1)			Transference number (± 0.02)	
	Nyquist plot	Conductivity spectra	DC 4-probe	Ionic (t_i)	Electronic (t_e)
NMC	9.12×10^{-6}	9.31×10^{-6}	1.12×10^{-5}	0.56	0.44
NMCD	4.96×10^{-6}	4.83×10^{-6}	5.04×10^{-6}	0.54	0.46
NMCG	2.13×10^{-6}	2.31×10^{-6}	2.45×10^{-6}	0.53	0.47
NMCH	1.81×10^{-6}	1.73×10^{-6}	1.98×10^{-6}	0.51	0.49

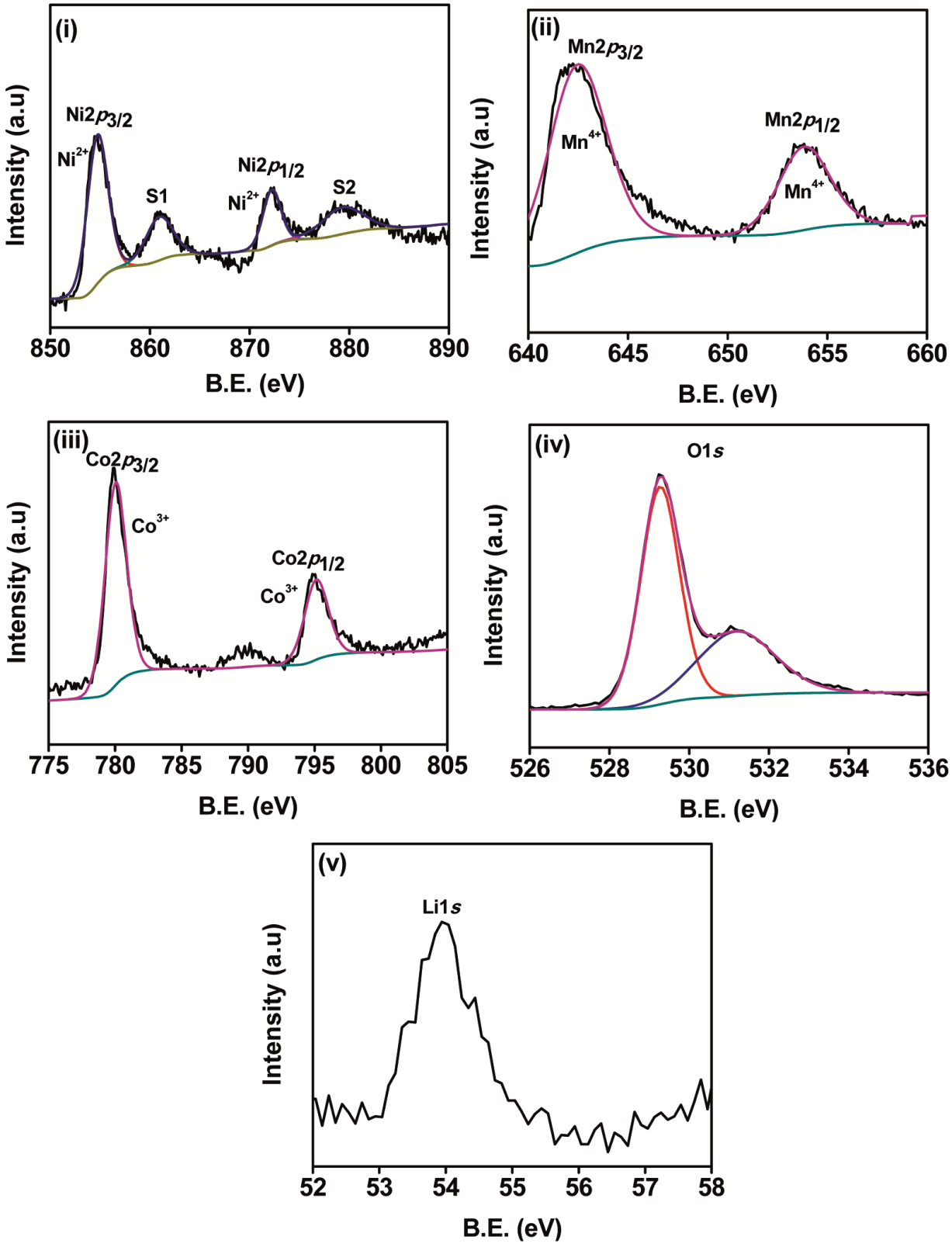

Fig. 8(a) — XPS spectra of NMC (i) Ni2*p*, (ii) Mn2*p*, (iii) Co2$p_{3/2}$, (iv) O1*s* and (v) Li1*s* peaks. (copyright permission from Elsevier Ref .23).

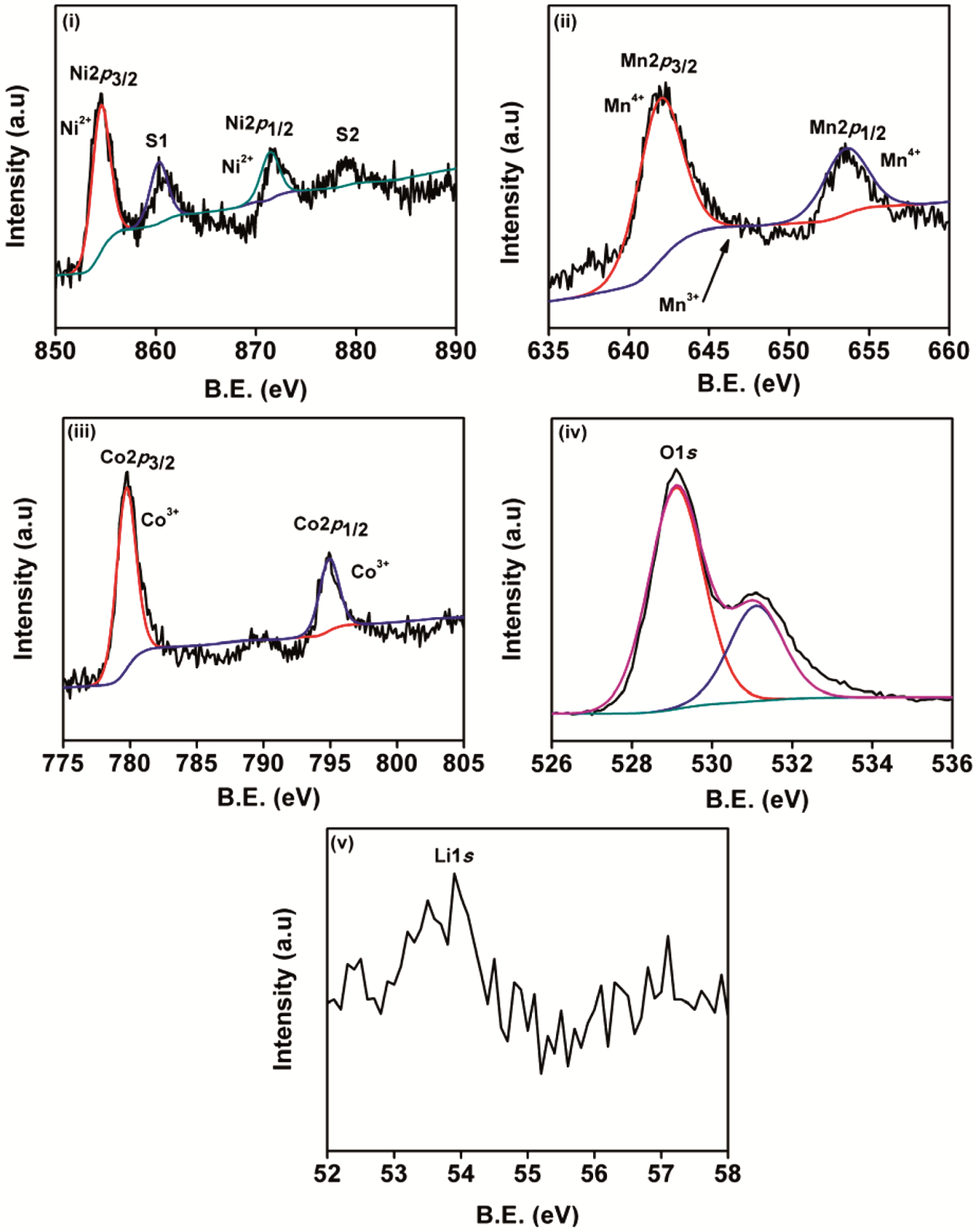

Fig. 8(b) — XPS spectra of NMCD (i) Ni2p, (ii) Mn2p, (iii) Co2$p_{3/2}$, (iv) O1s and (v) Li1s peaks.

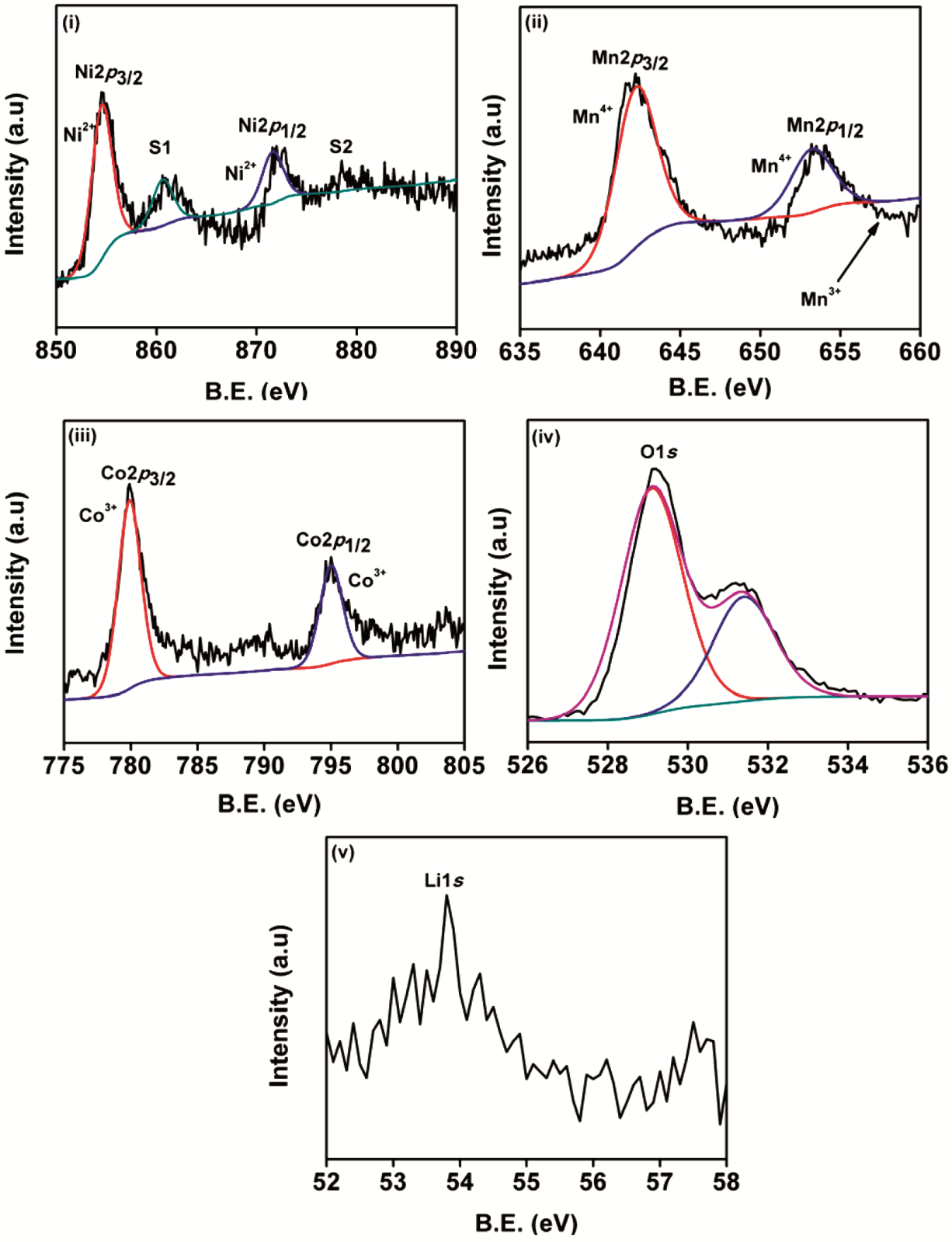

Fig. 8(c) — XPS spectra of NMCG (i) Ni2*p*, (ii) Mn2*p*, (iii) Co2$p_{3/2}$, (iv) O1*s* and (v) Li1*s* peaks.

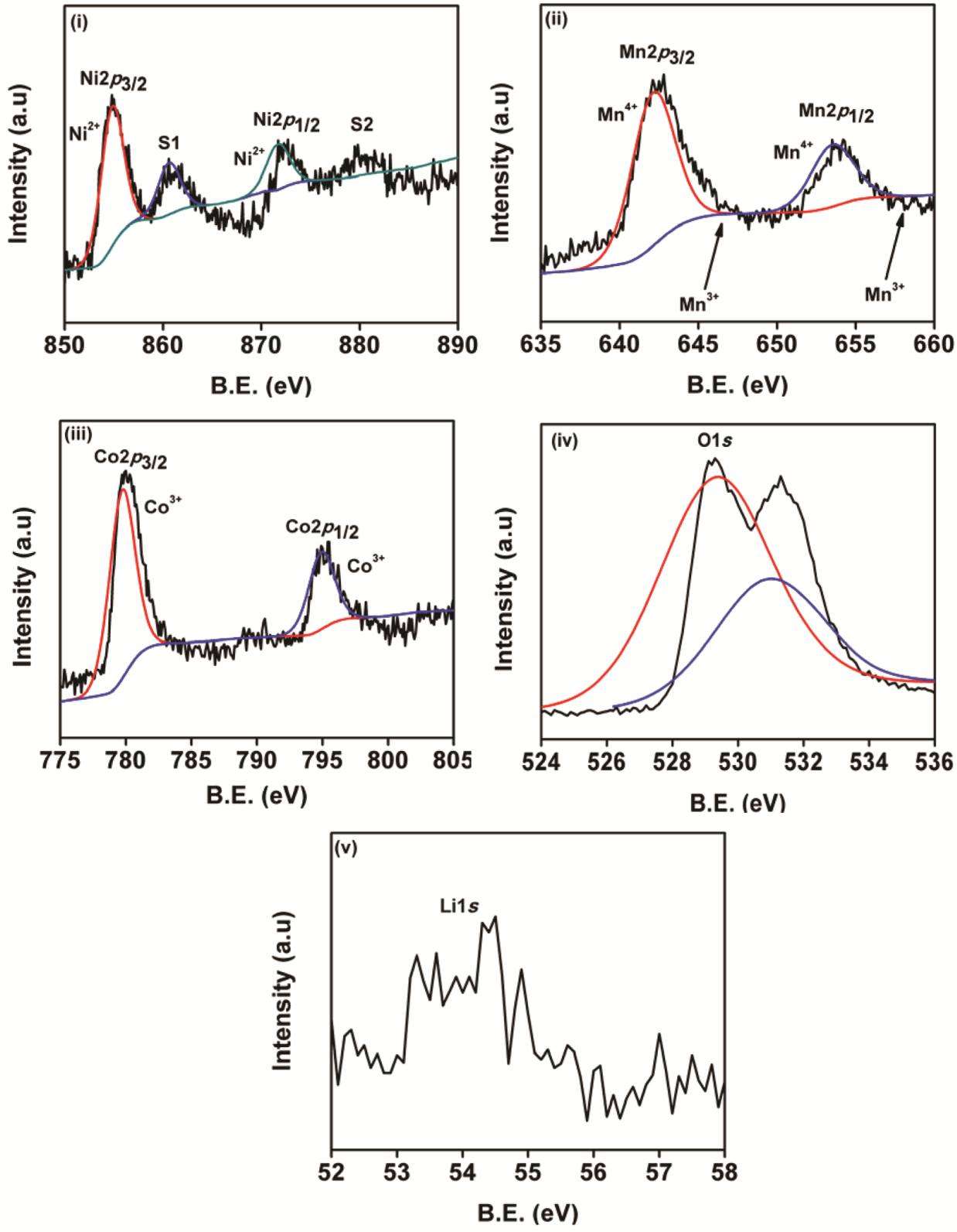

Fig. 8(d) — XPS spectra of NMCH (i) Ni2*p*, (ii) Mn2*p*, (iii) Co2$p_{3/2}$, (iv) O1*s* and (v) Li1*s* peaks.

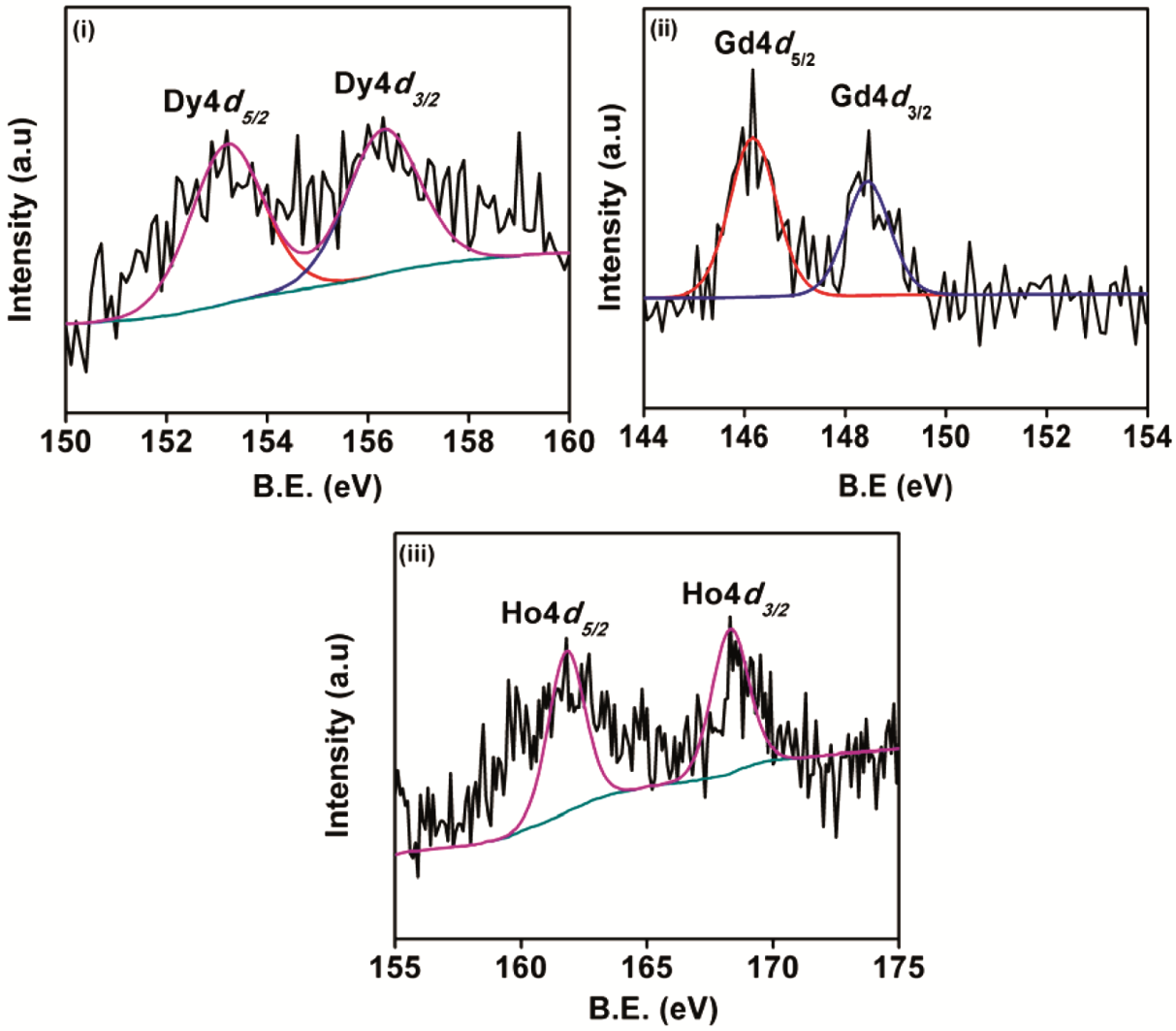

Fig. 8(e) — XPS spectra of (i) Dy4*d*, (ii) Gd4*d* and (iii) Ho4*d* peaks.

NMCG and NMCH, the weak signal (indicated by arrow marks in the XPS spectra of (Mn2$p_{3/2}$)) was observed at 647 and 658 eV, which was attributed to the presence of Mn^{3+} ions. The negligible presence of Mn^{3+} ions were identified in the CV plot. This validates our measurements. The ratio between Ni^{2+}/Ni^{3+} was found to be 95:05 for the sample NMC, whereas it was found to be 90:10, 88:12 and 80:20 for the samples NMCD, NMCG and NMCH, respectively. The higher in Ni^{2+}/Ni^{3+} ratio resulting in higher discharge capacity due to the better lithium intercalation and deintercalation as discussed in charge discharge analysis.

Conclusion

In summary, bare and rare earth doped $Li_{1.10}(Ni_{0.32}X_{0.01}Co_{0.33}Mn_{0.33})O_2$ (X = Dy/Gd/Ho) compounds were prepared by microwave assisted solvothermal route. Rietveld refined XRD patterns have shown the layered stacking arrangements of the atoms in a lattice point which were enhanced by rare earth doping. The unit cell volume of the compound $Li_{1.10}$ ($Ni_{0.32}$ $X_{0.01}Co_{0.33}Mn_{0.33}$)$O_2$ was expanded by doping owing to the higher ionic radii of dopants. SEM images have shownthat the doped compounds have higher particle size/agglomeration than the pristine compound. Raman scattering spectra confirmed the layered hexagonal structure of the $Li_{1.10}$ ($Ni_{0.32}X_{0.01}$ $Co_{0.33}Mn_{0.33}$) O_2 (X = Dy/Gd/Ho) compounds through the presence of active $A_{1g}$and E_g modes. The prepared coin cells were tested for its electrochemical performance at different voltage windows of 2.5 - 4.4/4.6/4.8 V at 0.2C rate. The parent compound $Li_{1.10}(Ni_{0.33}$

$Co_{0.33}Mn_{0.33})O_2$ delivered first cycle discharge capacity of 197 mAh/g in the potential window of 2.5-4.6 V. The capacity retention of was identified to be 93 % after 40th cycle. The exclusive reason for the highest discharge capacity was due to lower particle size of 288 nm and its higher conductivity of 9.12×10^{-6} S/cm. The parent compound $Li_{1.10}(Ni_{0.33}Co_{0.33}\ Mn_{0.33})O_2$ delivered discharge capacity of 163 mAh/g at the end of 50th cycle. Among the three rare earth doped compounds, $Li_{1.10}(Ni_{0.32}Dy_{0.01}\ Co_{0.33}Mn_{0.33})O_2$ delivered highest specific capacity of 166 mAh/g at the end of fiftieth cycle with 100 % capacity retention. Irrespective of dopants, all the doped compounds were found to be valuable in terms of electrochemical cycling stability even at higher potential window. The reason for the excellent cycling stability of the doped compounds was identified to be better mixed conducting nature than the parent compound under investigation. Overall, the present work reveals that the further optimization of the doping level, doping sites and choice of dopants is necessary in order to improve the electrochemical performance and the work is underway.

Acknowledgements

One of the author AS sincerely thanks the Science and Engineering Research Board (SERB)-Department of Science and Technology (DST), Government of India, New Delhi (Project No. EMR/2017/003227) dated 16 July 2018, for the funding. The authors thank Karunya Institute of Technology and Sciences, Coimbatore 641 114, Tamil nadu, India for the financial support through seed money project and for research facilities. The authors MVR, RPR and SA sincerely thank to the National Research Foundation, Prime Minister's Office, Singapore under its Competitive Research Programme (CRP Award No. NRF-CRP 10-2012-6,NRF-CRP 8-2011-4) for the research support.

References

1 Hu M, Pang X & Zhou Z, *J Power Sources*, 237 (2013) 229.
2 Kraytsberg A & Ein-Eli Y, *Adv Energy Mater*, 2 (2012) 9229.
3 Xing L Y, Hu M, Tang Q, Wei J P, Qin X & Zhou Z, *Electrochim Acta*, 59 (2012) 172.
4 Li H, Jin J, Wei J P, Zhou Z & Yan J, *Electrochem Commun*, 11 (2009) 95.
5 Li J, Baggetto L, Martha S K, Veith G M, Nanda J, Liang C & Dudney N J, *Adv Energy Mate*r, 3 (2013) 1275.
6 Hu M, Tian Y, Su L, Wei J & Zhou Z, *ACS Appl Mater Interfaces*, 5 (2013) 12185.
7 Hu M, Tian Y, Wei J, Wang D & Zhou Z, *J Power Sources*, 247 (2014) 794.
8 Yin S C, Grondey H, Strobel P, Huang H & Nazar L F,*J Am Chem Soc*, 125 (2003) 326.
9 Reddy M V, Mauger A, Julien C M, Paolella A & Zaghib K, *Mater*, 13 (2020) 1884.
10 Ren M, Zhou Z, Li Y, Gao X P & Yan J, *J Power Sources*, 162 (2006) 1357.
11 Reddy M V, Subba Rao G V & Chowdari B V R, *J Power Sources*, 159 (2006) 263.
12 Hu M, Wei J, Xing L & Zhou Z, *J Power Sources*, 222 (2013) 373.
13 Ohzuku T & Makimura M, *Chem Lett*, 30 (2003) 642.
14 Liu J, Chen L, Hou M, Wang F, Che R & Xia Y, *J Mater Chem*, 22 (2012) 25380.
15 Li X, Wei Y J, Ehrenberg H, Du F, Wang C Z & Chen G, *Solid State Ionics*, 178 (2008) 1969.
16 Periyasamy P, Kalaiselvi N & Kim H S, *Int J Electrochem Sci*, 2 (2007) 689.
17 Whittingham M, *Chem Rev*, 104 (2004) 4271.
18 Ceder G, Aydinol M K & Kohan A F, *Comp Mater Sci*, 8 (1997) 161.
19 Levasseur S, Menetrier M, Suard E & Delmas C, *Solid State Ionics*, 128 (2000) 11.
20 Myung S T, Komaba S & Kumagai N, *Solid State Ionics*, 170 (2004) 139.
21 Shlyakhtin O A, Choi S H, Yoon Y S & Oh Y J, *J Power Sources*, 141 (2005) 122.
22 Todorov Y M & Numata K, *Electrochim Acta*, 50 (2004) 495.
23 Senthil Kumar P, Sakunthala A, Prasada Rao R, Adams S, Chowdari B V R & Reddy M V, *Mater Res Bull*, 93 (2017) 381.
24 Ding Y, Zhang P, Jiang Y & Gao D, *Solid State Ionics*, 178 (2007) 967.
25 Zhang S, Wang Y, Liu J, Wan K & Lu F, *J Rare Earths*, 29 (2011) 891.
26 Ding Y, Zhang P & Jiang Y, *J Rare Earths*, 25 (2007) 268.
27 Fujii Y, Miura H, Suzuki N, Shoji T & Nakayama N, *J Power Sources*, 171 (2007) 894.
28 Deng C, Liu L, Zhou W, Sun K & Sun D, *Electrochim Acta*, 53 (2008) 2441.
29 Cao X, Zhao Y, Zhu L, Xie L, Cao X, Xiong S & Wang C, *Int J Electrochem Sci*, 11 (2016) 5267.
30 He Y S, Ma Z S, Liao X Z & Jiang Y, *J Power Sources*, 163 (2007) 1053.
31 Senthil K P, Sakunthala A, Reddy M V, Shanmugam S & Prabu M, *J Solid State Electrochem*, 20 (2016) 1865.
32 Selvasekarapandian S & Vijayakumar M, *Solid State Ionics*, 148 (2002) 329.
33 Liang L, Du K, Lu W, Peng Z, Cao Y & Hu G, *J Alloys Compd*, 613 (2014) 296.
34 Liu W, Wang M, Gao X L, Zhang W, Chen J & Zhou H, *J Alloys Compd*, 543 (2012) 181.
35 Li G, Huang Z, Zuo Z, Zhang Z & Zhou H, *J Power Sources*, 281 (2015) 69.
36 Li J, Xiong S, Liu Y, Ju Z & Qian Y, *Nano Energy*, 2 (2013) 1249.
37 Zhu H, Xie T, Chen Z, Li L, Xu M, Wang W, Lai Y & Lia J, *Electrochim Acta*, 135 (2014) 77.
38 Li D, Sasaki Y, Kobayakawa K & Sato Y, *Electrochim Acta*, 51 (2006) 3809.
39 Manikandan P & Periyasamy N, *Mater Res Bull*, 50 (2014) 132.
40 Huang H &Yang S, *J Phys Chem B*, 104 (2000) 1473.